Available online at www.sciencedirect.com

ScienceDirect

Procedia Engineering 10 (2011) 2478–2483

Engineering Procedia

ICM11

Evaluation of interfacial fracture toughness and friction coefficient in the single fiber fragmentation test

E. Graciani[a,*], J. Varna[b], V. Mantič[a], A. Blázquez[a], F. París[a]

[a]*University of Seville, Escuela Superior de Ingenieros, Camino de los Descubrimientos s/n, Sevilla 41092, Spain*
[b]*Luleå University of Technology, Luleå SE-97187, Sweden*

Abstract

Single fiber fragmentation test is extensively employed to characterize the fiber-matrix interface in composites. A novel technique for evaluating fracture toughness and friction coefficient at the fiber-matrix interface in an epoxy sample containing a single glass fiber is proposed. Using experimental measurements of the average fragment and debond lengths, Boundary Element (BE) models of the portion of sample corresponding to the average fiber fragment are created for increasing values of the applied strain. From the solution of the BE models, energy release rate (ERR) during crack propagation is evaluated using a Fracture Mechanics based approach which accounts for fiber-matrix interfacial friction. The calculated evolution of the ERR has a reasonably linear dependency on the applied strain, with a decreasing slope for increasing values of the interfacial friction coefficient. Since debond growth is stable, ERR should equal the interfacial fracture toughness during debond propagation. Consequently, interfacial friction coefficient and fracture toughness can be simultaneously determined by parametrically varying the friction coefficient until a null slope is obtained in the linear fit of the numerical solution of the ERR as a function of the applied strain. The applicability of the proposed technique is demonstrated with experimental results taken from the literature.

Keywords: composite materials, interfacial fracture toughness, interfaccial friction, Boundary Element Method.

1. Introduction

Among the wide range of composite materials that are used nowadays fiber reinforced composites are one of the most extended for building primary structures subjected to high loads. A typical composite of

* Corresponding author. Tel.: +34 954 487 299; fax: +34 954 461 637.
E-mail address: graciani@esi.us.es.

 doi:10.1016/j.proeng.2011.04.408

this kind is formed by a continuous matrix (usually constituted by a polymeric resin) and a fibrous reinforcement (mainly carbon or glass fibers) distributed within it.

Fiber reinforced composite materials are typically designed to work in the direction of the fibers, being their failure properties in this case mainly controlled by the strength properties of the fibers. However, the existence of differently oriented plies in the laminates and the presence of impact loads, which produce stresses transferred along many directions within the laminate, are responsible for the appearance of failure mechanisms in which the failure properties of the matrix and the interface play a fundamental role.

Since it was introduced by Kelly and Tyson [1], single fiber fragmentation test (SFFT) has been extensively used for characterization of the fiber-matrix interface. The main objective of the present study is to introduce a novel technique for data reduction in the SFFT which enables the simultaneous determination of the interfacial friction coefficient and the interfacial mode II fracture toughness.

This novel data reduction technique employs the near-tip elastic solution in a typical debond crack, evaluated numerically using the Boundary Element Method (BEM), to determine the energy release rate (ERR) associated to debond propagation, taking into account the frictional contact along crack faces and the possible interaction with the debond crack growing in the opposite side of the fiber fragment [2].

To obtain the evolution of the near-tip solution, a set of BEM models are built using the data measured during the experiments. The experimental data employed in the present work (the evolution of the debond length and the fragment length with the applied load) have been obtained from the literature [3,4].

2. Experimental data

The experimental work was carried out using E-glass single fiber composites (Kim and Nairn [3,4]). All specimens used a transparent epoxy matrix which enabled observation of the fragmentation process with an optical microscope. To measure debond lengths, the specimens were observed using photoelasticity while under load [3,4].

Relevant material properties of the E-glass fiber and the epoxy matrix (taken from [3,4]) are listed in Table 1. SFFT samples were oven cured at 100 K above room temperature.

Table 1. Material properties

Property	E-Glass	Epoyy
Outer radius (r_f or r_m in μm)	7	1000
Young's modulus (E_f or E_m in GPa)	72.5	2.6
Poisson's ratio (ν_f or ν_m)	0.2	0.34
Thermal expansion coefficient (α_f or α_m in ppm/K)	5.4	40

Since the cross section of the sample is much larger than the cross section of the fiber, the actual shape of the cross section is not relevant for the stress analysis. A circular sample cross section has been employed since it enables assuming axial symmetry, thus simplifying the stress analysis.

Experimental measurements of the debond length, a, and the crack density (taken from [3,4]) are shown in Fig. 1. In the form as data are presented in Fig. 1, the strain dependent debond length and fragment length data for given individual SFFT specimen cannot be identified. Nevertheless calculations have to be performed for specified fragment length, debond length and applied strain. To overcome this problem, the crack density data has been averaged, and the evolution of the fragment length, L_f, with the applied strain has been obtained from the continuous line shown in Fig. 1(b).

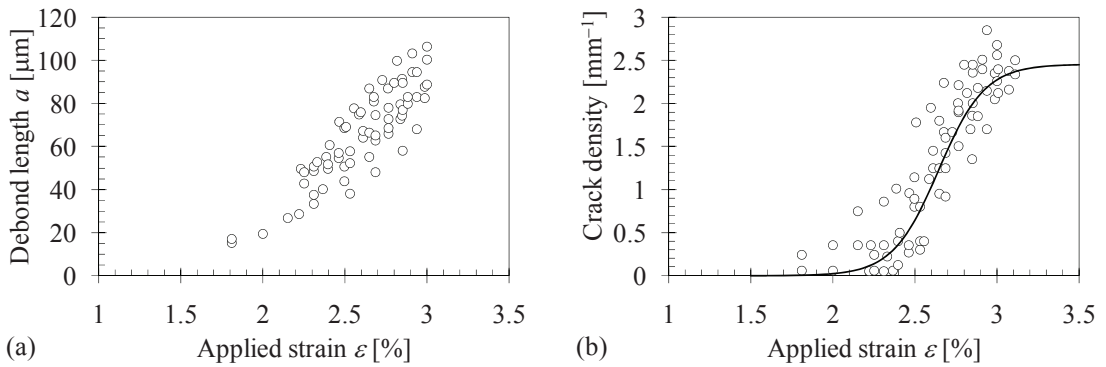

Fig. 1. Experimental measurements of: (a) debond length; (b) fiber crack density.

3. Numerical model

The main assumptions made in the numerical analysis are [2]: linear elastic isotropic behavior of the constituents, axial symmetry (with respect to the fiber axis) and periodicity of the solution in the vicinity of all fragment ends (which implies local symmetry with respect to the plane containing the fiber crack). With these assumptions, the model employed is the one shown in Fig. 2(a), in which the main dimensions and the boundary conditions are indicated. It has to be emphasized that the model employed in this paper consists in the radial section of the portion of sample corresponding to one half of a fiber fragment. Therefore, the debond length a and the fragment length L_f are in fact the semi-debond length and semi-fragment length if compared with those defined in [3,4].

As can be seen, both mechanical and thermal loads are defined to take into account the thermal residual stresses [2]. The average elongation considered in the model ε_0 is equal to the sum of the mechanically applied strain ε and the thermal shrinkage $\varepsilon_{\Delta T} \approx \alpha_m \Delta T_0 \approx -0.4\%$ as correspond to the decrease of temperature $\Delta T_0 = -100$ K from the solidification temperature to room temperature.

Numerical analysis is carried out using a self-developed numerical tool, based on BEM, which takes into account the frictional contact between crack faces [5,6]. For each configuration, defined by the experimental values of a and L_f at a certain applied strain ε, a sequence of models are created which only differ in the interfacial friction coefficient μ which is not known *a priori*.

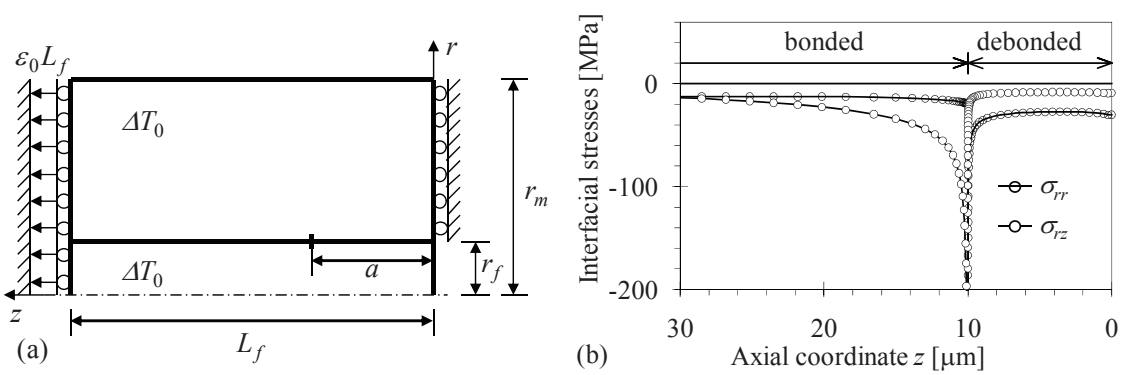

Fig. 2. (a) sketch of the model and boundary conditions; (b) near-tip solution of interfacial stresses.

Note that pre-existing fiber and debond cracks are considered and that both mechanical and thermal loads are applied simultaneously, thus neglecting the effect of load history in the solution of the frictional contact problem. Previous analysis, in which the BEM solution is compared with FEM solutions using non-linear analysis and cohesive elements (following the actual load history of the sample), confirm the validity of this assumption [7].

With the numerical tool employed [5] only the boundaries of the model shown in Fig. 2(a) need to be meshed. Continuous linear elements, with two nodes in the extremes of the elements have been employed, thus a high mesh refinement in the vicinity of the crack tips being extremely easy to carry out.

An example of the near-tip stress solution is shown in Fig. 2(b), were the normal $\sigma_{zz}(r_f, z)$ and tangential $\sigma_{rz}(r_f, z)$ components of the tractions along the interface are shown. The asymptotic behavior of the elastic solution along the interface in the vicinity of the debond crack tip satisfies:

$$\sigma_{rz}(r_f, a+\rho) \sim \rho^{\lambda-1},\ \sigma_{rz}(r_f, a-\rho) \sim \rho^{\lambda-1} \text{ and } \Delta u_z(r_f, a-\rho) \sim \rho^{\lambda}, \tag{1}$$

where $\sigma_{rz}(r_f, a+\rho)$ are the singular shear stresses ahead of the crack tip, $\sigma_{rz}(r_f, a-\rho)$ are the singular shear stresses along crack faces and $\Delta u_z(r_f, a-\rho)$ are the relative displacements (sliding) between the crack faces, with ρ being the distance to the crack tip. According to Comninou [8], singularity order λ depends upon bimaterial Dundur's parameter β and the interfacial friction coefficient μ, being defined by the following relation: $\tan(\lambda\pi) = (\mu\beta)^{-1}$.

4. Evaluation of the mode II energy release rate

Since the debond crack is closed and compressed along its whole length, see Fig. 2(b), crack growth occurs in pure fracture mode II. ERR associated to crack growth is evaluated with a local approach, in which only the near-tip elastic solution along the interface is employed. To that end, the *initial* situation (denoted in the following by a − superscript) in which the debond crack length is a, is compared with the *final* situation (denoted in the following by a + superscript) in which the debond crack length is $a + \Delta a$. Both situations are indicated in Fig. 3(a).

The procedure employed for evaluation of ERR can be considered divided in two stages. In the first stage, the crack is virtually extended a finite length Δa while the interfacial stresses $\sigma_{rz}^{-}(r_f, a+\Delta a-\rho)$, with $0 < \rho < \Delta a$, are substituted by identical external virtual stresses. Therefore, during this stage no change should be observed in the elastic solution of the problem which is identical to the *initial* situation.

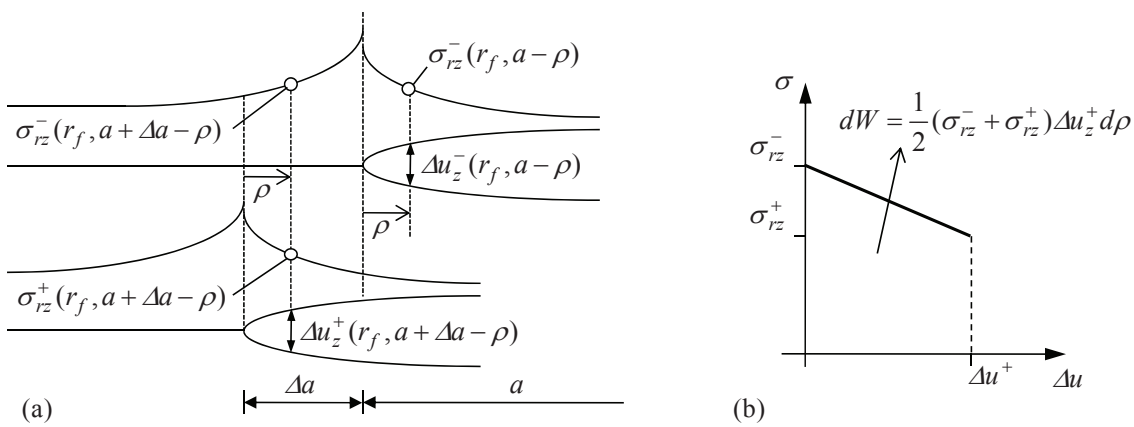

Fig. 3. (a) sketch of the model and boundary conditions; (b) near-tip solution of interfacial stresses.

In the second stage, at each interfacial point in the range $a < z < a + \Delta a$, the external virtual stresses are linearly transformed into the stresses $\sigma_{rz}^{+}(r_f, a + \Delta a - \rho)$. Therefore, at the end of the second stage the situation is identical to the *final* situation. Consequently, the work carried out by the virtual stresses during the second stage should be equal to the energy released during the crack growth.

The work carried out by the virtual stresses at each point is indicated in Fig. 3(b). Integrating along the virtual crack extension yields:

$$G_{II}(\Delta a)\Delta a = \frac{1}{2}\int_0^{\Delta a} [\sigma_{rz}^{-}(r_f, a + \Delta a - \rho) + \sigma_{rz}^{+}(r_f, a + \Delta a - \rho)]\, \Delta u_z^{+}(r_f, a + \Delta a - \rho)\, d\rho\,, \tag{2}$$

where $G_{II}(\Delta a)\Delta a$ is the energy released during a finite crack extension of length Δa.

Assuming that $\Delta a << a$, the near-tip solution in the *final* situation can be considered identical to the near-tip solution in the *initial* situation. Therefore equation (2) is transformed into:

$$G_{II}(\Delta a) = \frac{1}{2\Delta a}\int_0^{\Delta a} [\sigma_{rz}^{-}(r_f, a + \Delta a - \rho) + \sigma_{rz}^{-}(r_f, a - \rho)]\, \Delta u_z^{-}(r_f, a - \rho)\, d\rho\,. \tag{3}$$

As can be seen this expression is similar to the one employed for evaluation of mode II ERR using VCCT. However, two clear distinctions have to be emphasized. First, a new term appears, $\sigma_{rz}^{-}(r_f, a - \rho)$, which is a consequence of the fact that, after crack growth, the crack faces are not free of stresses. The second, and more important, difference is that, as a consequence of the asymptotic behavior shown in (1), $G_{II}(\Delta a) \sim \Delta a^{2\lambda - 1}$ and, consequently, it vanishes when $\Delta a \to 0$. Therefore, finite crack extensions (instead of infinitesimal) have to be considered to determine the ERR in presence of interfacial friction. In this paper a constant finite crack extension of $\Delta a = 1\,\mu\text{m}$ has been employed. In a previous analysis [7] it has been shown that when this Δa value is used, results obtained with the present approach are in a very good agreement with results obtained employing cohesive zone formulations.

5. Determination of the mode II fracture toughness

Computed results of ERR $G_{II}(\Delta a)$ are shown in Fig. 4(a). As mentioned above, each experimental measurement yields the debond length a and fragment length L_f at a certain applied strain ε. Using each couple of values of a and L_f, a sequence of BEM models, in which only the interfacial friction coefficient is varied, are solved to determine the near-tip elastic solution. $G_{II}(\Delta a)$ is then evaluated introducing this BEM solution into equation (3). With this procedure, the evolution of $G_{II}(\Delta a)$ with the applied strain is numerically obtained for each of the assumed values of the friction coefficient μ. As can be seen in Fig. 4(a), for each value of μ, $G_{II}(\Delta a)$ has a distinct linear dependency upon the applied strain, being the slope decreasing with increasing values of μ.

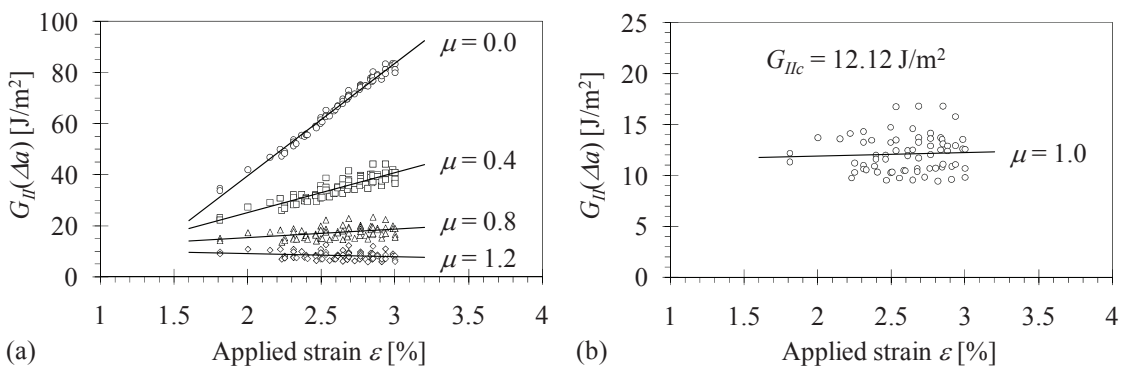

Fig. 4. Simulated evolutions of the ERR: (a) results for distinct friction coefficients; (b) best fit with a horizontal line.

The debond crack growth takes place when the ERR equals the mode II interfacial fracture toughness G_{IIc}, i.e. the propagation criterion $G_{II}(\Delta a) = G_{IIc}$ is fulfilled during crack growth. Consequently, since the models have been constructed using experimental measurements of $a(\varepsilon)$ and $L_f(\varepsilon)$, the evolution of the computed values of $G_{II}(\Delta a)$ should be a horizontal line. Thus, the actual value of the friction coefficient is the one which provides a linear evolution of $G_{II}(\Delta a)$ with null slope, and the average value of $G_{II}(\Delta a)$ is the value of G_{IIc}.

In view of the results shown in Fig. 4(a), new models are created in order to carry out a fine tune of the interfacial friction coefficient. The best fit, yielding an interfacial friction coefficient $\mu = 1.0$ and a mode II interfacial fracture toughness $G_{IIc} = 12.12$ J/m^2, is shown in Fig. 4(b).

6. Concluding remarks

A novel technique for evaluating fiber-matrix interfacial friction coefficient and mode II interfacial fracture toughness from experimental measurements obtained with the single fiber fragmentation test has been proposed and demonstrated using test data taken from the literature.

The proposed technique employs the average values of the fragment length and the debond length, measured in the test, to build a sequence of BEM models which enable the calculation of the energy released during crack propagation, taking into account the interfacial friction and the interaction with the debond crack existing at the opposite end of the fragment. Interfacial friction coefficient and mode II interfacial fracture toughness are simultaneously obtained seeking for the value of the friction coefficient which yields a constant energy release rate during debond growth.

Acknowledgements

This work has been partially funded by project P08-TEP-04051 (Proyecto de Excelencia de la Junta de Andalucía).

References

[1] Kelly A, Tyson WR. Tensile properties of fiber-reinforced metals: copper/tungsten and copper/molybdenum. *J Mech Phys Solids* 1965;13:329-50.

[2] Graciani E, Mantič V, París F, Varna J. Numerical analysis of debond propagation in the single fibre fragmentation test. *Compos Sci Technol* 2009;69:2514-20.

[3] Kim BE, Nairn JA. Observations of fiber fracture and interfacial debonding phenomena using the fragmentation test in single fiber composites. *J Compos Mater* 2002;36:1825-57.

[4] Kim BE, Nairn JA. Experimental verification of the effects of friction and residual stress on the analysis of interfacial debonding and toughness in single fiber composites. *J Mater Sci* 2002;37:3965-72.

[5] Graciani E, Mantič M, París F, Blázquez A. Weak formulation of axi-symmetric frictionless contact problems with boundary elements: Application to interface cracks. *Comput Struct* 2005;83:836-55.

[6] Graciani E, Mantič V, París F. BEM solution of axi-symmetric contact problems by weak application of contact conditions with non conforming discretizations. In: Aliabadi MH, editor. *Boundary Element Techniques*, Queen Mary and Westfiel College; 1999, p. 445-54.

[7] Graciani E. Numerical analysis of the single fiber fragmentation test including the effect of interfacial friction. *Doctoral Thesis*, Luleå University of Technology, 2010.

[8] Comninou M. Interface crack with friction in the contact zone. *J Appl Mech-T ASME* 1977;44:780-71.